Rieske Clusters Hot Paper

International Edition: DOI: 10.1002/anie.201506788
German Edition: DOI: 10.1002/ange.201506788

Biomimetic [2Fe-2S] Clusters with Extensively Delocalized Mixed-Valence Iron Centers

*Shenglai Yao, Florian Meier, Nils Lindenmaier, Robert Rudolph, Burgert Blom, Mario Adelhardt, Jörg Sutter, Stefan Mebs, Michael Haumann, Karsten Meyer, Martin Kaupp, and Matthias Driess**

In memory of Heinrich Nöth

Abstract: *A complete series of biomimetic [2Fe-2S] clusters, $[(L^{Dep}Fe)_2(\mu\text{-}S)_2]$ (**3**, $L^{Dep} = CH[CMeN(2,6\text{-}Et_2C_6H_3)]_2$), $[(L^{Dep}Fe)_2(\mu\text{-}S)_2K]$ (**4**), $[(L^{Dep}Fe)_2(\mu\text{-}S)_2][Bu_4N]$ (**5**, Bu = n-butyl), and $[(L^{Dep}Fe)_2(\mu\text{-}S)_2K_2]$ (**6**), could be synthesized and characterized. The all-ferric [2Fe-2S] cluster **3** is readily accessible through the reaction of $[(L^{Dep}Fe)_2(\mu\text{-}H)_2]$ (**2**) with elemental sulfur. The chemical reduction of **3** with one molar equivalent of elemental potassium affords the contact ion pair $K^+[2Fe\text{-}2S]^-$ (**4**) as a one-dimensional coordination polymer, which in turn reacts with $[Bu_4N]Cl$ to afford the separate ion pair $[Bu_4N]^+[2Fe\text{-}2S]^-$ (**5**). Further reduction of **4** with potassium furnishes the super-reduced all-ferrous [2Fe-2S] cluster **6**. Remarkably, complexes **4** and **5** are [2Fe-2S] clusters with extensively delocalized $Fe^{2+}Fe^{3+}$ pairs as evidenced by ^{57}Fe Mössbauer, X-ray absorption and emission spectroscopy (XAS, XES) and in accordance with DFT calculations.*

Binuclear, rhomboidal iron–sulfur clusters [2Fe-2S], such as those in in ferredoxin- and Rieske-type proteins, are ubiquitous biological cofactors in nature.[1] The most important function of these clusters is based on one-electron transfer processes of the [2Fe-2S] moiety, which thus shuttles between the all-ferric $[2Fe\text{-}2S]^{2+}$ and the mixed-valence $[2Fe\text{-}2S]^{1+}$ states.[1b] The electrons of the $Fe^{2+}Fe^{3+}$ pair in the $[2Fe\text{-}2S]^{1+}$ site are usually localized and antiferromagnetically (AF) coupled to give a valence-trapped $S = 1/2$ ground state. Remarkably, single cysteine/serine mutations of coordinating residues lead to a valence-delocalized $S = 9/2$ $[2Fe\text{-}2S]^{1+}$ state along with the $S = 1/2$ $[2Fe\text{-}2S]^{1+}$ state.[2] Moreover, [2Fe-2S] units constitute the building blocks of all Fe-S clusters, and valence-delocalized $[2Fe\text{-}2S]^{1+}$ fragments are intrinsic components of all high-nuclearity Fe-S clusters in at least one oxidation state.[1,2] Therefore, the study of biomimetic [2Fe-2S] clusters, especially towards the development of delocalized mixed-valence $[2Fe\text{-}2S]^{1+}$ systems, continues to attract much attention. A number of biomimetic [2Fe-2S] clusters have emerged,[3] most of which, however, are all-ferric [2Fe-2S] cluster models. Synthetic analogues of the mixed-valence $[2Fe\text{-}2S]^{1+}$ clusters have previously only been generated by electrochemical methods[4a] or by in situ chemical reduction, and they were only investigated spectroscopically in solution.[4b] In 1993, Gibson and Beardwood described an isolable $[2Fe\text{-}2S]^{1+}$ system, which was only characterized by ^{57}Fe Mössbauer spectroscopy.[4c] Very recently, Meyer and coworkers synthesized a whole series of [2Fe-2S] clusters, including a $[2Fe\text{-}2S]^{1+}$ and a $[2Fe\text{-}2S]^{0}$ cluster.[5a,b] Meanwhile, they also reported structurally characterized biomimetic Rieske $[2Fe\text{-}2S]^{2+}$ and $[2Fe\text{-}2S]^{1+}$ clusters.[5c–e] Thus far, all synthetic mixed-valence $[2Fe\text{-}2S]^{1+}$ clusters contain only partially delocalized iron pairs. Herein, we present the facile synthesis of a series of $[2Fe\text{-}2S]^n$ clusters ($n = 2+, 1+, 0$) that are supported by a β-diketiminato ligand ($L^{Dep} = CH[CMeN(2,6\text{-}Et_2C_6H_3)]_2$), including $[2Fe\text{-}2S]^{1+}$ clusters with an extensively delocalized $Fe^{2+}Fe^{3+}$ pair.

The $[2Fe\text{-}2S]^n$ clusters can be straightforwardly accessed from the dinuclear β-diketiminato iron(II) hydride precursor **2** (Scheme 1), which was prepared from β-diketimine **1**[6] in 68% yield. Its single-crystal structure exhibits a dimer that is very similar to the known β-diketiminato iron hydride $[(L^{tBu}Fe)_2(\mu\text{-}H)_2]$ ($L^{tBu} = CH[CtBuN(2,6\text{-}iPr_2C_6H_3)]_2$; Figure 1, left).[7] Treatment of **2** with 1/4 molar equivalents of S_8 in toluene afforded complex **3** almost quantitatively with concomitant liberation of dihydrogen (Scheme 1). Complex **3** could be isolated as a dark brown solid in 87% yield. The formation of **3** was rather unexpected as the reaction of $[(L^{Dipp}Fe)_2(\mu\text{-}N_2)]$ ($L^{Dipp} = CH[CMeN(2,6\text{-}iPr_2C_6H_3)]_2$) with sulfur furnishes the monosulfide complex $[(L^{Dipp}Fe)_2(\mu\text{-}S)]$ in high yield.[8] The molecular structure of **3**, which was established by X-ray diffraction, features a $[Fe_2(\mu\text{-}S)_2]$ core coordinated by two β-diketiminato ligands, forming a strongly puckered C_3N_2Fe six-membered ring (Figure 1, right). The structural parameters of the $[Fe_2S_2]$ core are similar to those

[*] Dr. S. Yao, Dipl.-Chem. F. Meier, M.Sc. N. Lindenmaier, Dipl.-Chem. R. Rudolph, Dr. B. Blom, Prof. Dr. M. Kaupp, Prof. Dr. M. Driess
Technische Universität Berlin
Institut für Chemie, Sekr. C2
Strasse des 17. Juni 135, 10623 Berlin (Germany)
E-mail: matthias.driess@tu-berlin.de
Dipl.-Chem. M. Adelhardt, Dr. J. Sutter, Prof. Dr. K. Meyer
Lehrstuhl für Anorganische und Allgemeine Chemie
Department Chemie und Pharmazie
Friedrich-Alexander-Universität Erlangen-Nürnberg (FAU)
Egerlandstrasse 1, 91058 Erlangen (Germany)
Dr. S. Mebs, Priv.-Doz. Dr. M. Haumann
Freie Universität Berlin, Fachbereich Physik
Arnimallee 14, 14195 Berlin (Germany)
Supporting information and ORCID(s) from the author(s) for this article are available on the WWW under http://dx.doi.org/10.1002/anie.201506788.

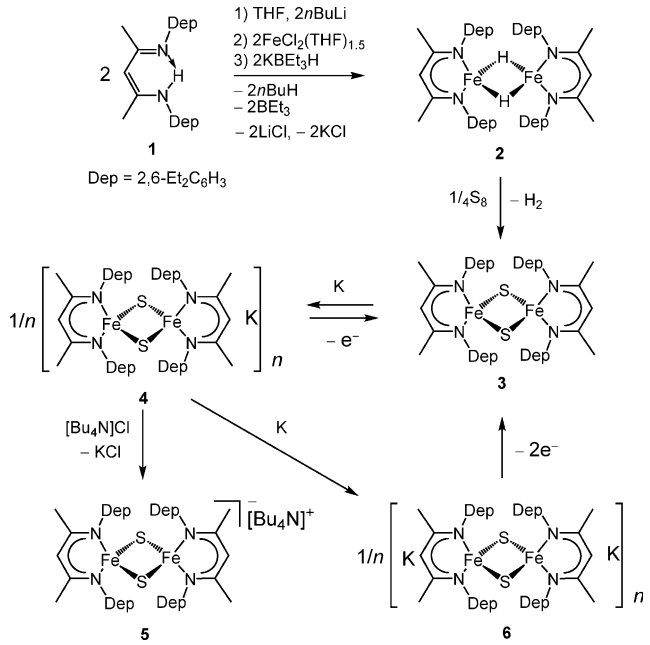

Scheme 1. Synthesis of complexes **2**–**6** from **1**.

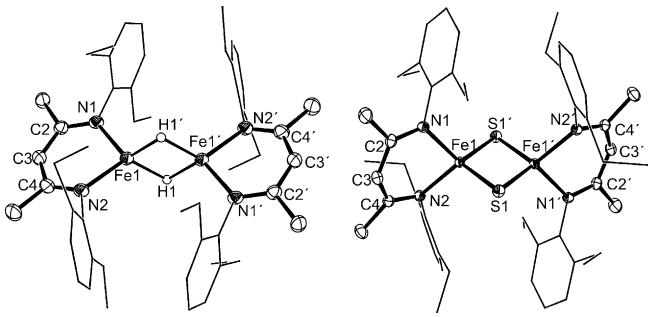

Figure 1. Molecular structures of **2** (left) and **3** (right). Ellipsoids set at 50% probability. Hydrogen atoms (except for H1 and H1′) are omitted for clarity. Symmetry transformations used to generate equivalent atoms with (′) in **2**: $-x+1,-y+2,-z$ and in **3**: $-x+1/2,-y+1/2,-z$. Selected distances (Å) for **2**: Fe1–N1 1.990(2), Fe1–N2 1.995(2), Fe1–Fe1′ 2.6347(9); for **3**: Fe1–N1 1.996(1), Fe1–N2 2.012(1), Fe1–S1′ 2.1813(5), Fe1–S1 2.2057(5), Fe1–Fe1′ 2.6792(5), S1–Fe1′ 2.1813(5).

of a synthetic $[2Fe\text{-}2S]^{2+}$ cluster supported by a bis(benzimidazolato) ligand.[5a] The ^1H NMR spectrum recorded in $[D_6]$benzene at room temperature shows six resonances that are paramagnetically shifted (Supporting Information, Table S14). Magnetic susceptibility measurements of **3** in benzene solution revealed a magnetic moment of 1.09 μ_B at 298 K. A solid-state SQUID measurement revealed a temperature-dependent effective magnetic moment (Figure S21). The μ_{eff} value increased from 0.15 to 1.57 μ_B as the temperature was increased from 2 to 290 K, indicating a strong antiferromagnetic interaction between both ferric ions with $S=5/2$. The coupling constant J was determined to be $-209\ cm^{-1}$ ($H=-2JS_A\cdot S_B$). Furthermore, complex **3** was analyzed by ^{57}Fe Mössbauer spectroscopy at 80 K (Figure 2). The zero-field Mössbauer spectrum shows one quadrupole doublet with an isomer shift of $\delta=0.29\ mm\,s^{-1}$ and a quadrupole splitting of $\Delta E_Q=1.06\ mm\,s^{-1}$, confirming the presence of high-spin Fe^{III} centers in an environment of covalently bound ligands. These values are akin to those observed for other all-ferric $[2Fe\text{-}2S]^{2+}$ clusters.[3]

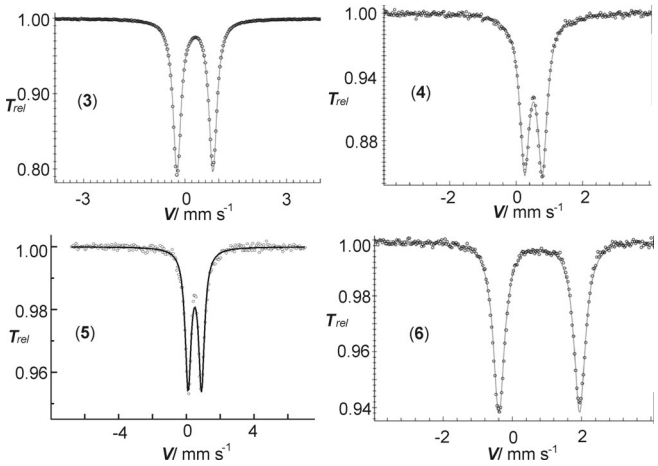

Figure 2. Zero-field ^{57}Fe Mössbauer spectra of **3**, **4**, **5**, and **6** recorded at 80 K. The solid lines are fits with Lorentzian doublets to the experimental values using the following isomer shifts and quadrupole splittings: $\delta=0.29\ mm\,s^{-1}$, $\Delta E_Q=1.06\ mm\,s^{-1}$ for **3**; $\delta=0.52\ mm\,s^{-1}$, $\Delta E_Q=0.53\ mm\,s^{-1}$ for **4**; $\delta=0.50\ mm\,s^{-1}$, $\Delta E_Q=0.79\ mm\,s^{-1}$ for **5**; $\delta=0.77\ mm\,s^{-1}$, $\Delta E_Q=2.34\ mm\,s^{-1}$ for **6**.

The electrochemical properties of **3** were investigated by cyclic voltammetry (CV, in THF solutions at 295 K; Figures S1–S6). A reversible redox process was observed at $E=-1.45$ V versus Fc/Fc^+ ($Fc=[Fe(C_5H_5)_2]$), as well as a quasi-reversible electrode process at $E=-2.55$ V, which is possibly followed by a chemical reaction or a structural change. This corresponds to the formation of the mixed-valence and the all-ferrous [2Fe-2S] clusters, respectively. Accordingly, treatment of **3** with one molar equivalent of potassium in THF at room temperature afforded $[(L^{Dep}Fe)_2(\mu\text{-}S)_2K]$ (**4**), which was isolated in 59% yield as dark brown crystals (Scheme 1). Complex **4** crystallized as a one-dimensional polymer linked by the potassium ions. Despite the coordinated potassium ions, the structure of the $[(L^{Dep}Fe)_2(\mu\text{-}S)_2]^-$ moiety is reminiscent of its precursor **3**. However, slight elongations can be observed for the Fe–N (2.035(2) and 2.044(2) Å in **4** vs. 1.996(1) and 2.012(1) Å in **3**) and the Fe–S distances (2.2177(8) and 2.2504(8) Å in **4** vs. 2.1813(5) and 2.2057(5) Å in **3**). The same is true for the Fe···Fe (2.7087(8) Å in **4** vs. 2.6792(5) Å in **3**) and the S···S distances (3.554 Å in **4** vs. 3.474 Å in **3**).

Surprisingly, the zero-field ^{57}Fe Mössbauer spectrum of **4**, recorded at 80 K, shows only one quadrupole doublet with $\delta=0.52\ mm\,s^{-1}$ and $\Delta E_Q=0.53\ mm\,s^{-1}$ (Figure 2). The isomer shift of $\delta=0.52\ mm\,s^{-1}$, which is intermediate between the values expected for the ferric and the ferrous iron in an $Fe^{2+}Fe^{3+}$ localized mixed-valence pair,[2c] suggests a delocalization, at least on the time scale of the measurement (for ^{57}Fe Mössbauer spectroscopy ca. 10^{-7} s). The latter value is very close to that observed for the delocalized $S=9/2$ $[2Fe\text{-}2S]^{1+}$ component that was obtained by cysteine/serine mutations ($\delta=0.50\ mm\,s^{-1}$, 4.2 K).[2b] It is noteworthy that diiron com-

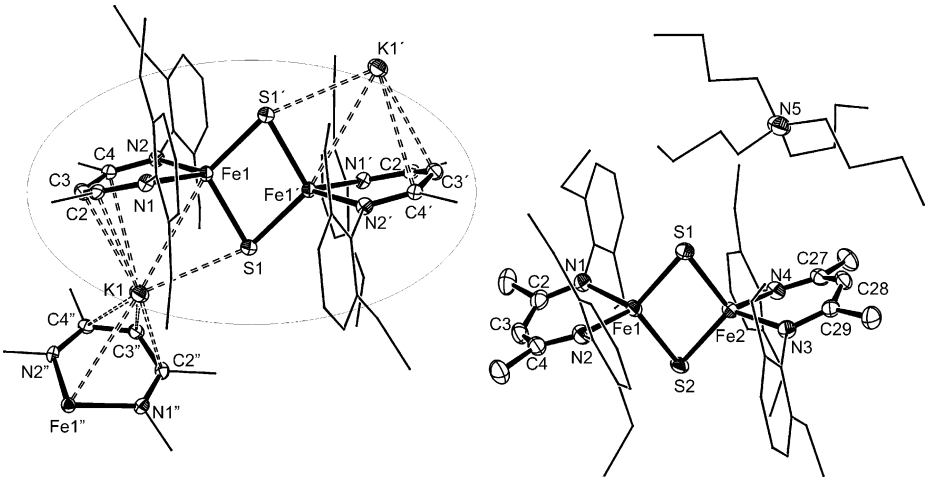

Figure 3. Molecular structure of **4** (left, cut from the one-dimensional polymeric structure; K1′, Fe1″, N1″, C2″, C3″, C4″, and N2″ belong to another molecule unit) and **5** (right). Ellipsoids set at 50% probability. Hydrogen atoms are omitted for clarity. Symmetry transformations used to generate equivalent atoms with (′): $-x,-y+1,-z$; with (″): $-x,y,-z+1/2$. Selected distances (Å) for **4**: Fe1–N2 2.035(2), Fe1–N1 2.044(2), Fe1–S1′ 2.2177(8), Fe1–S1 2.2504(8), Fe1–Fe1′ 2.7087(8); for **5**: Fe1–N1 2.036(2), Fe1–N2 2.049(2), Fe1–S1 2.2152(5), Fe1–S2 2.2335(5), Fe1–Fe2 2.6894(4), S1–Fe2 2.2272(5), Fe2–N3 2.042(2), Fe2–N4 2.045(2), Fe2–S2 2.2161(5).

plexes with fully delocalized $Fe^{2.5+}Fe^{2.5+}$ cores are generally quite rare.[9] The X-band EPR spectrum of **4**, which was recorded in frozen THF solutions at 12 K (Figure S24), however, corresponds to a rhombic structure with g values of 2.06, 1.95, and 1.73, which is characteristic for an $S=1/2$ system. The average g value of 1.91 is in agreement with the values reported for the Rieske centers and the model compounds ($g_{av}=1.91$ and 1.92, respectively).[10a–c] Magnetic susceptibility measurements of **4**, also in [D_8]THF solution, revealed a μ_{eff} value of 2.44 μ_B at 298 K. Moreover, the SQUID magnetization measurement showed a temperature-dependent effective magnetic moment, which increased from 2.6 to 3.4 μ_B with an increase in temperature from 2 to 300 K (Figure S22).

The metathesis reaction of **4** with [Bu_4N]Cl afforded [$(L^{Dep}Fe)_2(\mu\text{-}S)_2$][$Bu_4N$] (**5**), which was isolated in 88% yield (Scheme 1). Single-crystal X-ray diffraction revealed the anticipated separate ion pair **5** (Figure 3, right). The structural parameters of the [Fe_2S_2] core in **5** are very similar to those of anion **4**. Likewise, the zero-field ^{57}Fe Mössbauer spectrum of **5**, recorded at 80 K, shows only one quadrupole doublet, with an isomer shift and quadrupole splitting very similar to those observed for **4** (**4**: $\delta=0.52$, $\Delta E_Q=0.53$ mm s^{-1} vs. **5**: $\delta=0.50$, $\Delta E_Q=0.79$ mm s^{-1}; Figure 2). The magnetic moment of a microcrystalline sample of complex **5** was determined to be 1.73 μ_B at 2 K, and is temperature-independent up to 80 K (Figure S23). With increasing temperature, the moment increased from 1.8 to 2.3 μ_B at room temperature. In agreement with the observed spin-only value for one unpaired electron, the X-band EPR spectrum of **5** in frozen THF solutions at 8 K shows, similar to that of **4**, a signal characteristic for an $S=1/2$ system with g values of 1.77, 1.97, and 2.07 ($g_{av}=1.94$; Figure S25).

Strikingly, the mixed-valence iron centers in **5** can be distinguished by ^{57}Fe Mössbauer spectroscopy at low temperature with an applied magnetic field. While the zero-field ^{57}Fe Mössbauer spectrum of **5** recorded at 4 K (Figure S28) still shows only one quadrupole doublet, different parameters ($\delta=0.57$ mm s^{-1}, $\Delta E_Q=1.17$ mm s^{-1}) and significant broadening were observed, which could be explained by changes in the spin dynamics and electron hopping in the mixed-valence diiron pair. In fact, the Mössbauer spectrum of **5** with an applied magnetic field of $B=2$ T (Figure S29 and S30) confirmed that the Fe^{2+} and Fe^{3+} ions are distinguishable from each other already at 60 K. Furthermore, no intervalence bands, indicative of a fully delocalized $Fe^{+2.5}Fe^{+2.5}$ pair belonging to Robin–Day class III,[10d] could be detected in the investigated range of the UV/Vis/NIR spectrum (Figure S20). In other words, the two iron centers in **5** show the phenomenon of temperature-dependent mixed valency within the time scale of Mössbauer spectroscopy. Moreover, on the much faster time scale of XAS and XES (ca. 10^{-14} s), the mixed-valence iron pairs in **4** and **5** are extensively delocalized (see below).

XAS/XES measurements were employed to further characterize the electronic structures of the series **2**, **3**, **4**, and **5** (Figures S31–S35).[11] Small differences in the XANES (X-ray absorption near edge structure) and EXAFS (extended X-ray absorption fine structure) structures between **4** and **5** reproduced the small geometry changes for the two counterions in the crystals. The pronounced intensity of the $K_{\beta'}$ spin-polarization signal in the non-resonantly excited K_β main-line emission ($3p\rightarrow1s$) spectra revealed exclusively high-spin (h.s.) Fe ions in all complexes, which was confirmed by the lack of $K_{\beta'}$ emissions in the resonantly excited spectra. Similar $K_{\beta'}$ features for complexes **3**, **4**, and **5** indicated similar effective unpaired Fe(d) spin states and thus delocalization of the surplus charge in **4** and **5**. The pre-edge absorption in the XANES structure probes resonant 1s electron transitions (core-to-valence excitation, c2v) into unoccupied molecular orbitals (MOs; e.g., with Fe(d) character), whereas the K_β satellite emission ($K\beta_{2,5}$) probes electronic relaxation to the 1s core hole (valence-to-core decay, v2c) from occupied MOs (e.g., with ligand(s,p) character), thus providing benchmark data for electronic structure calculations. Such c2v and v2c spectra were collected experimentally (Figures S33 and S34) and also calculated by DFT (BP86/TZVPP). The calculated spectra are only in excellent agreement with the experiment ones for ferromagnetically coupled h.s. Fe^{2+} ions in paramagnetic complex **2**, for the antiferromagnetically coupled h.s. Fe^{3+} ions in complex **3**, as well as for the h.s. mixed-valence Fe sites in the $S=1/2$ state of complexes **4** and **5**. The data revealed

significant delocalization of occupied Fe(d)-character MOs over both Fe ions (v2c), but a more asymmetric localization of the unoccupied Fe(d)-character MOs (c2v), whereas for the ligand-dominated MOs, this trend was reversed. This results in spectrally distinguishable contributions from the two Fe ions and their ligands to the electronic transitions, accounting even for the minor spectral differences between **4** and **5**. The XAS/XES analysis supports extensive, but not complete, valence level delocalization in complexes **4** and **5**, which is slightly, but detectably diminished for complex **4** compared to **5** owing to the intimate interaction with the potassium counterion.

The electrochemical properties of **4** and **5** were also studied by cyclic voltammetry, suggesting the reduction of the anion to be feasible (Figure S7–S17). Accordingly, further reduction of **4** with potassium mirror resulted in a green precipitate of $[(L^{Dep}Fe)_2(\mu\text{-}S)_2K_2]$ (**6**) in 49% yield (Scheme 1). Compound **6** is insoluble in THF and other common aprotic organic solvents. As expected, treatment of **6** with two equivalents of $[Cp_2Fe][B(C_6H_3(CF_3)_2)_4]$ or an excess of elemental sulfur in THF led to the formation of **3**. The zero-field ^{57}Fe Mössbauer spectrum of **6** shows one quadrupole doublet with $\delta = 0.77\ mm\,s^{-1}$ and $\Delta E_Q = 2.34\ mm\,s^{-1}$ (at 80 K), indicating the presence of two h.s. Fe^{2+} sites (Figure 2). These values are comparable to those observed for the super-reduced forms of the [2Fe-2S] ferredoxin and Rieske proteins.[12] The parameters of **6** are also rather close to those observed by Meyer et al. for the super-reduced biomimetic [2Fe-2S] cluster ($\delta = 0.79\ mm\,s^{-1}$ and $\Delta E_Q = 2.67\ mm\,s^{-1}$ at 6 K).[5b]

Structure optimizations (B3LYP-D3(BJ)/basis-1; for computational details see the Supporting Information) of **3** and its monoanion $\mathbf{3}^-$ and dianion $\mathbf{3}^{2-}$ in ferromagnetically coupled h.s. and antiferromagnetically coupled broken-symmetry (b.s.) configurations are qualitatively in good agreement with the X-ray diffraction data (Table S10). For the neutral complex **3**, the computations at this level of theory (using the Yamaguchi spin-projection formula)[13] gave an antiferromagnetic Heisenberg coupling constant of $J = -217\ cm^{-1}$ (Table S11), which is in excellent agreement with the SQUID data. The computed spin-density distributions (Tables S12 and S18) corroborate the similarities to the all-ferric states of ferredoxin and Rieske-type $[2Fe\text{-}2S]^{2+}$ clusters. Whereas the spin density is appreciably delocalized onto the bridging sulfides in the h.s. state, the delocalization is partially interrupted by the antiferromagnetic coupling in the b.s. configuration. This is a known consequence of super-exchange in iron–sulfur clusters.[14–16,10d] More importantly, the optimized structure for $\mathbf{3}^-$, which contains a mixed-valence $[2Fe\text{-}2S]^{1+}$ core, deviates very little from a symmetric structure, suggesting a strongly delocalized mixed-valence system. Notably, this holds for both the h.s. and b.s. configurations. Although the spin densities of the b.s. state exhibit a slight inequality between the two halves of the complex (Table S12 and S18), interpretation in terms of a localized mixed-valence system does not appear to be warranted here, also in view of the almost symmetric NPA charge distribution (Table S13). Even if there might be two identical minima deviating from an idealized symmetry, there does not seem to be a notable barrier. Interestingly, even in the b.s. state, the spin-density distribution exhibits appreciable delocalization over the bridging sulfides (Tables S12 and S18) in spite of the antiferromagnetic coupling, and much more so than for the neutral or dianionic complexes.

The structure of the super-reduced dianion $\mathbf{3}^{2-}$ (i.e., the anion of compound **6**) was optimized at the same computational level, again for the h.s. and b.s. states. As might be expected, the predicted structure for this all-ferrous complex features an even more expanded coordination set for the iron centers and also an even longer S···S distance than the mixed-valence monoanion $\mathbf{3}^-$ (Table S10). Delocalization of the spin density onto the sulfide bridges is less pronounced than for the monoanion and comparable to the situation in the all-ferric complex **3** (Tables S12 and S18).

In summary, a complete series of biomimetic $[2Fe\text{-}2S]^n$ clusters supported by a β-diketiminato ligand (**3**: $n = 2+$; **4**, **5**: $n = 1+$; **6**: $n = 0$) have been synthesized starting from the diiron(II) dihydride precursor **2**. Magnetic measurements revealed strong antiferromagnetic coupling of the two Fe centers in the respective [2Fe-2S] clusters. Remarkably, the mixed-valence clusters **4** and **5** are extensively delocalized $[2Fe\text{-}2S]^{1+}$ clusters with $Fe^{2+}Fe^{3+}$ sites as suggested by ^{57}Fe Mössbauer and XAS/XES spectroscopic data and in accordance with results from DFT calculations. The facile synthesis of these [2Fe-2S] clusters, especially of the extensively delocalized mixed-valence [2Fe-2S] clusters **4** and **5**, may lead to their application in redox catalysis and could improve our fundamental understanding of the reactivity of [2Fe-2S] clusters with respect to selective one-electron transfer for small-molecule activation.

Acknowledgements

We are grateful to the Cluster of Excellence UniCat for financial support (EXC 314-2, supported by the Deutsche Forschungsgemeinschaft (DFG)). M.A. and K.M. acknowledge financial support from the Friedrich-Alexander-University Erlangen-Nürnberg. M.H. thanks the DFG (Ha3263/6-2 and Heisenberg fellowship) and the BMBF (05K14KE1) for financial support and the group of P. Glatzel (ID26 at ESRF) for technical assistance. We thank Dr. Eckhard Bill (MPI Mülheim) for some of the Mössbauer and SQUID measurements and valuable discussions.

Keywords: iron · mixed-valence compounds · Rieske clusters · sulfur · β-diketiminato ligands

How to cite: *Angew. Chem. Int. Ed.* **2015**, *54*, 12506–12510
Angew. Chem. **2015**, *127*, 12686–12690

[1] a) H. Beinert, R. H. Holm, E. Münck, *Science* **1997**, *277*, 653; b) E. I. Solomon, X. Xie, A. Dey, *Chem. Soc. Rev.* **2008**, *37*, 623.
[2] a) B. R. Crouse, J. Meyer, M. K. Johnson, *J. Am. Chem. Soc.* **1995**, *117*, 9612; b) C. Achim, M.-P. Golinelli, E. Bominaar, J. Meyer, E. Münck, *J. Am. Chem. Soc.* **1996**, *118*, 8168; c) C. Achim, E. Bominaar, J. Meyer, J. Peterson, E. Münck, *J. Am. Chem. Soc.* **1999**, *121*, 3704; d) S. Subramanian, E. C. Duin,

S. E. J. Fawcett, F. A. Armstrong, J. Meyer, M. K. Johnson, *J. Am. Chem. Soc.* **2015**, *137*, 4567.
[3] P. V. Rao, R. H. Holm, *Chem. Rev.* **2003**, *104*, 527.
[4] a) P. K. Mascharak, G. C. Papaefthymiou, R. B. Frankel, R. H. Holm, *J. Am. Chem. Soc.* **1981**, *103*, 6110; b) P. Beardwood, J. F. Gibson, *J. Chem. Soc. Dalton Trans.* **1992**, 2457; c) X.-Q. Ding, E. Bill, A. X. Trautwein, H. Winkler, A. Kostikas, V. Papaefthymiou, A. Simopoulos, P. Beardwood, J. F. Gibson, *J. Chem. Phys.* **1993**, *99*, 6421.
[5] a) A. Albers, S. Demeshko, S. Dechert, E. Bill, E. Bothe, F. Meyer, *Angew. Chem. Int. Ed.* **2011**, *50*, 9191; *Angew. Chem.* **2011**, *123*, 9357; b) A. Albers, S. Demeshko, K. Pröpper, S. Dechert, E. Bill, F. Meyer, *J. Am. Chem. Soc.* **2013**, *135*, 1704; c) A. Albers, T. Bayer, S. Demeshko, S. Dechert, F. Meyer, *Chem. Eur. J.* **2013**, *19*, 10101; d) J. Ballmann, A. Albers, S. Demeshko, S. Dechert, E. Bill, E. Bothe, U. Ryde, F. Meyer, *Angew. Chem. Int. Ed.* **2008**, *47*, 9537; *Angew. Chem.* **2008**, *120*, 9680; e) A. Albers, S. Demeshko, S. Dechert, C. T. Saouma, J. M. Mayer, F. Meyer, *J. Am. Chem. Soc.* **2014**, *136*, 3946.
[6] D. J. E. Spencer, A. M. Reynolds, P. L. Holland, B. A. Jazdzewski, C. Duboc-Toia, L. L. Pape, S. Yokota, Y. Tachi, S. Itoh, W. B. Tolman, *Inorg. Chem.* **2002**, *41*, 6307.
[7] J. M. Smith, R. J. Lachicotte, P. L. Holland, *J. Am. Chem. Soc.* **2003**, *125*, 15752.
[8] J. Vela, S. Stoian, C. J. Flaschenriem, E. Münck, P. L. Holland, *J. Am. Chem. Soc.* **2004**, *126*, 4522.
[9] a) S. Drüeke, P. Chaudhuri, K. Pohl, K. Wieghardt, X.-Q. Ding, E. Bill, A. Sawaryn, A. X. Trautwein, H. Winkler, S. J. Gurman, *J. Chem. Soc. Chem. Commun.* **1989**, 59; b) C. Ercolani, S. Hewage, R. Heucher, G. Rossi, *Inorg. Chem.* **1993**, *32*, 2975.
[10] a) J. A. Fee, K. L. Findling, T. Yoshida, R. Hille, G. E. Tarr, D. O. Hearshen, W. R. Dunham, E. P. Day, T. A. Kent, E. Münck, *J. Biol. Chem.* **1984**, *259*, 124; b) P. Bertrand, B. Guigliarelli, J. P. Gayda, P. Beardwood, J. F. Gibson, *Biochim. Biophys. Acta Protein Struct. Mol. Enzymol.* **1985**, *831*, 261; c) M. Orio, J. M. Mouesca, *Inorg. Chem.* **2008**, *47*, 5394; d) M. B. Robin, P. Day, *Adv. Inorg. Chem. Radiochem.* **1968**, *10*, 247.
[11] a) C. Lambertz, P. Chernev, K. Klingan, N. Leidel, K. G. Siegfridsson, T. Happe, M. Haumann, *Chem. Sci.* **2014**, *5*, 1187; b) P. Chernev, C. Lambertz, A. Brunje, N. Leidel, K. G. Sigfridsson, R. Kositzki, C. H. Hsieh, S. Yao, R. Schiwon, M. Driess, C. Limberg, T. Happe, M. Haumann, *Inorg. Chem.* **2014**, *53*, 12164.
[12] a) S. J. Yoo, J. Meyer, E. Münck, *J. Am. Chem. Soc.* **1999**, *121*, 10450; b) E. J. Leggate, E. Bill, T. Essigke, G. M. Ullmann, J. Hirst, *Proc. Natl. Acad. Sci. USA* **2004**, *101*, 10913.
[13] S. Yamanaka, T. Kawakami, H. Nagao, K. Yamaguchi, *Chem. Phys. Lett.* **1994**, *231*, 25.
[14] L. Noodleman, C. Y. Peng, D. A. Case, J. M. Mouesca, *Coord. Chem. Rev.* **1995**, *144*, 199.
[15] L. Noodleman, D. A. Case, J. M. Mouesca, B. Lamotte, *J. Biol. Inorg. Chem.* **1996**, *1*, 177.
[16] H. Beinert, *J. Biol. Inorg. Chem.* **2000**, *5*, 2.

Received: July 23, 2015
Published online: September 3, 2015

